Ultrasonics 54 (2014) 1720–1728

Contents lists available at ScienceDirect

Ultrasonics

journal homepage: www.elsevier.com/locate/ultras

High-frequency guided ultrasonic waves for hidden defect detection in multi-layered aircraft structures

Bernard Masserey [a], Christian Raemy [a], Paul Fromme [b,*]

[a] Department of Mechanical Engineering, University of Applied Sciences, 1705 Fribourg, Switzerland
[b] Department of Mechanical Engineering, University College London, London WC1E 7JE, United Kingdom

ARTICLE INFO

Article history:
Received 30 August 2013
Received in revised form 3 April 2014
Accepted 23 April 2014
Available online 5 May 2014

Keywords:
Multilayer
Guided ultrasonic waves
Hidden defect

ABSTRACT

Aerospace structures often contain multi-layered metallic components where hidden defects such as fatigue cracks and localized disbonds can develop, necessitating non-destructive testing. Employing standard wedge transducers, high frequency guided ultrasonic waves that penetrate through the complete thickness were generated in a model structure consisting of two adhesively bonded aluminium plates. Interference occurs between the wave modes during propagation along the structure, resulting in a frequency dependent variation of the energy through the thickness with distance. The wave propagation along the specimen was measured experimentally using a laser interferometer. Good agreement with theoretical predictions and two-dimensional finite element simulations was found. Significant propagation distance with a strong, non-dispersive main wave pulse was achieved. The interaction of the high frequency guided ultrasonic waves with small notches in the aluminium layer facing the sealant and on the bottom surface of the multilayer structure was investigated. Standard pulse-echo measurements were conducted to verify the detection sensitivity and the influence of the stand-off distance predicted from the finite element simulations. The results demonstrated the potential of high frequency guided waves for hidden defect detection at critical and difficult to access locations in aerospace structures from a stand-off distance.

1. Introduction

During the service life of aerospace structures damage can occur due to cyclic loading conditions [1]. Common maintenance problems include disbonds of the sealant layers connecting multiple metallic sheets and the development of fatigue cracks. Such structures must therefore be regularly inspected non-destructively to detect hidden damage such as fatigue cracks before they have reached a critical length. Recently an ultrasonic-based structural health monitoring method has been developed for real time, in situ monitoring of cracks at fastener holes using an angle beam through transmission technique [2]. Standard bulk wave Ultrasonic Testing (UT) has a proven sensitivity for the detection of small defects, e.g., shear wave angle beam measurements [3]. However, it often necessitates local access and time-consuming scanning of the inspected part [4]. Rayleigh waves have been used for the detection of surface fatigue cracks in metallic plates [5]. Analytical models have been developed to describe the interaction of Rayleigh waves with surface cracks [6], as well as numerical simulations complemented by experimental results [7]. Typically damage detection using Rayleigh waves requires access to the side of the structure containing the defect.

Large areas of plate structures can be inspected and monitored from a single, remote access point using guided ultrasonic waves [8]. These are often used in a low frequency-thickness range below the cut-off frequency of the higher wave modes to simplify data interpretation [4]. However, the resulting wavelengths are typically significantly larger than in bulk wave UT, thus limiting the sensitivity for the detection of small defects [9]. The interaction of low frequency guided waves with small surface defects in plates has been studied using Finite Element (FE) simulations and experiments [10]. The propagation of guided ultrasonic waves in bonded components [11] and the interaction with holes in metallic plates has been investigated [12]. Low-frequency guided ultrasonic waves were used for the detection of fatigue cracks at fastener holes [13].

The application of guided ultrasonic wave modes in the higher frequency-thickness range has more recently been investigated

* Corresponding author. Tel.: +44 207 679 3944; fax: +44 207 388 0180.
E-mail addresses: bernard.masserey@hefr.ch (B. Masserey), p.fromme@ucl.ac.uk (P. Fromme).

http://dx.doi.org/10.1016/j.ultras.2014.04.023
0041-624X/

for non-destructive testing purposes. The S_0 mode (around 5 MHz mm) was used for corrosion detection in aircraft structures [14], and longitudinal modes (above 15 MHz mm) were employed for plate inspection [15]. This type of waves allows for the inspection of structures over reasonably long distances, and can be used even if local access to the inspected part is not possible [4]. The employed wavelengths are comparable to those commonly used in bulk wave UT, possibly allowing good sensitivity for the detection of small defects [15]. High frequency guided waves excited using standard 90° angle beam transducers at around 6.75 MHz mm can be interpreted as the superposition of the first anti-symmetric A_0 and symmetric S_0 Lamb wave modes [16]. These waves can propagate along the structure and allow for the inspection of both plate surfaces due to an energy transfer between the surfaces. A hybrid analytical/numerical model was developed to describe the wave propagation and the reflection at small surface defects in single layer metallic plates [17]. From standard pulse-echo measurements the location and damaged plate side of small surface defects in aluminium plates could be determined using a combination of time-of-flight and frequency evaluation of the reflected pulse [18]. Fatigue crack growth at a fastener hole in tensile, aluminium specimens was detected and monitored in situ using non-contact measurement of high frequency guided ultrasonic waves [19]. The detection of defects in the different layers of multi-layered aircraft structures is one of the requirements for future Structural Health Monitoring (SHM) systems [20]. A UT technique for 2nd layer defect detection has been developed using an angled phase-array probe and automated analysis of the acquired ultrasonic signals [21]. However, 2nd layer defect detection using conventional UT techniques can be problematic if the coupling medium (sealant) between the layers around the fastener hole is inadequate or missing [21]. Guided ultrasonic waves have energy distributed through the thickness of the multi-layered structure, making it in principle possible to inspect the different layers. Low frequency guided ultrasonic waves were employed to monitor fatigue crack growth at a fastener hole in a multi-layered structure [22]. The potential for the detection of real defects in an inaccessible layer was demonstrated, but a limited sensitivity for the detection of fatigue crack growth initiation was noted. The possibility of fatigue crack detection at fastener holes in multi-layered structures using high frequency guided ultrasonic waves (5 MHz) has been investigated [23]. It was shown that defect detection is possible, but that detection sensitivity depends on the interface conditions between the layers. It was also noted that high frequency guided ultrasonic waves are attenuated, if a material, such as an adhesive, is present between the metallic layers, making the monitoring of large areas more difficult.

In this contribution the potential of high frequency guided ultrasonic waves for the detection of hidden defects in multi-layered aerospace structures has been investigated. These waves can propagate over medium distances and are in principle sensitive for defect detection through the complete specimen thickness. The wave propagation characteristics of high frequency guided wave modes excited using a standard 90° angle beam wedge in a multi-layered model structure have been studied. The structure consists of two adhesively bonded aluminium plates with an epoxy based sealant layer [24]. Interference occurs between the wave modes during propagation along the structure, resulting in a frequency dependent variation of the energy through the thickness with distance. Finite Element (FE) simulations have been carried out and compared to laboratory measurements using a laser interferometer. The sensitivity for the detection of an internal notch at the sealant layer and on the bottom surface of the multilayer structure from a stand-off distance using pulse-echo (P/E) measurements has been demonstrated.

2. Experimental details

2.1. Specimen preparation

The multilayer structure model investigated in this contribution was made of two 3 mm thick aluminium plates with a width of 70 mm and a length of 600 mm connected with an approximately 0.25 mm thick epoxy based sealant layer, see Fig. 1. The plate material is an aluminium alloy 2014 T6 widely used for aerospace applications, having a Young's modulus of 73.1 GPa, Poisson's ratio of 0.33, and density of 2800 kg/m^3. The sealant is a two-part structural paste adhesive Hysol EA 9394 with a Young's modulus of 4.237 GPa (data from supplier), density of 1360 kg/m^3, and Poisson's ratio of 0.45. Measurements of the Young's modulus have been performed on a moulded 120 mm × 15 mm × 3 mm epoxy specimen in a standard tensile machine to confirm the material properties specified by the supplier. The relative error between the measured and the supplier value was below 1%. The thickness of the sealant layer was controlled by mixing approximately 4% volume fraction of spacer beads with a maximum diameter of 0.249 mm into the epoxy paste and clamping the specimen during curing at room temperature. To control the accuracy and the reproducibility of the sealant layer, the thicknesses of the different layers were measured along the centreline of the specimens in 1 mm step size using a coordinate measuring machine. The sealant thickness was obtained by subtraction of the aluminium thicknesses (measured before application of the epoxy paste) from the total multilayer thickness (measured after curing). The resultant thickness on the centreline was measured as varying between 0.22 mm and 0.28 mm, with an average sealant thickness of approximately 0.25 mm. Multiple specimens without defects were manufactured in order to investigate the high frequency guided ultrasonic wave generation and propagation in multilayer structures. More specimens were manufactured with an artificial defect. The notch was placed either in one of the aluminium plates at the interface between aluminium and sealant, as illustrated schematically in Fig. 1(b), or on the bottom surface of the multilayer structure. The notch was cut across the width of the specimen to a depth of 0.3 mm using an Electro-Discharge Machining (EDM) device. Restrictions of the EDM device imposed a notch width of approximately 0.4 mm and a maximum specimen length of 550 mm. The notch was placed at 150 mm from one end of the specimen. A wire covered with Teflon tape was placed into the notch to avoid sealant ingress during sealant application. The tape was removed after curing of the epoxy paste.

2.2. Measurement setup

The high frequency ultrasonic guided wave was generated on the surface of the multilayer specimen using a standard 1 MHz half inch transducer mounted on a 90° angle beam wedge for steel. The spatial period of the generated ultrasonic field at the interface wedge-aluminium can be evaluated on the basis of the Rayleigh wavelength: performing the calculation for the transducer centre frequency leads to a wavelength λ_R of 3.0 mm, about half the thickness of the multilayer specimen. The wedge was clamped on the specimen so that the main propagation axis is the centre line of the multilayer specimen, as displayed in Fig. 1(a).

For the investigation of the wave propagation characteristics a five cycle tone burst at 1 MHz centre frequency (sinusoid in a Hanning window) was generated in an arbitrary waveform generator and amplified using a broadband power amplifier. The out-of-plane component of the surface velocity was measured along the centre line of the specimen (step size: 1 mm) using a heterodyne laser interferometer mounted on a scanning rig. The origin ($x = 0$)

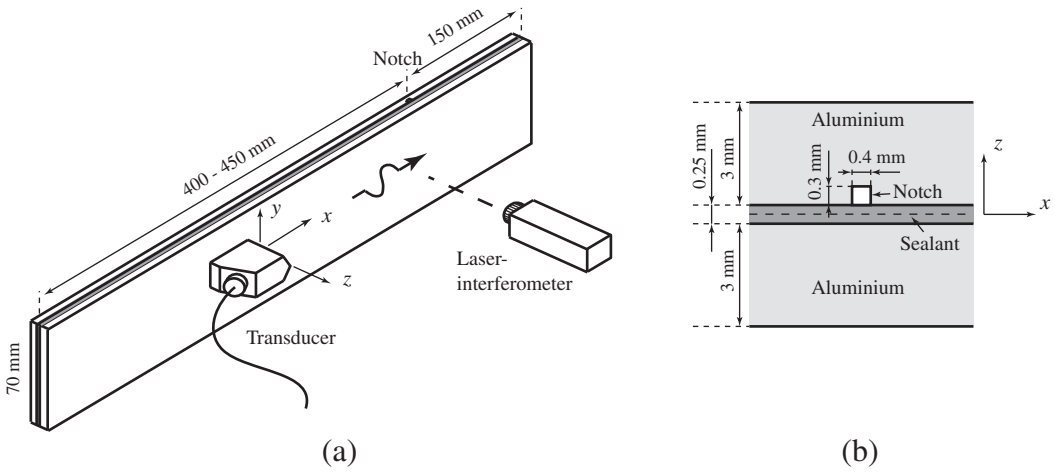

Fig. 1. (a) Schematic of experimental setup to measure wave propagation along multi-layer specimen (550–600 mm × 70 mm × 6.25 mm), excitation using 1 MHz 90° angle beam transducer, measurement using laser interferometer moved along line parallel to propagation direction. (b) detailed side view of multilayer cross-section (3 mm aluminium, 0.25 mm sealant, 3 mm aluminium) with EDM notch (0.3 mm × 0.4 mm).

was taken as the first point in front of the wedge. The output of the interferometer demodulator was bandpass filtered (0.5–1.5 MHz), averaged (100 averages) and saved using a digital oscilloscope. Additional scans were performed in front of the wedge on lines perpendicular to the main propagation direction in order to quantify and separate the effects of the beam spread of the angle-beam transducer and the material attenuation (mostly due to the sealant layer), both resulting in an amplitude decrease on the centre line of the specimen. The energy of the wave pulse propagating through each line was calculated by summing up the energy (and thus suppressing beam spread attenuation) and used to calculate the attenuation due to the material damping. The attenuation values were found as 4 Np/m for the beam spread and 1.5 Np/m for the material damping of the sealant.

The scattering at the hidden notches was investigated by means of pulse-echo measurements. The transducer was driven by a voltage spike generated by a standard ultrasonic pulser–receiver to allow for the P/E measurement using the inbuilt receiver circuitry. The wedge was placed on the specimen surface and measurements were taken in 10 mm intervals for stand-off distances ranging between 50 mm and 300 mm from the defect location.

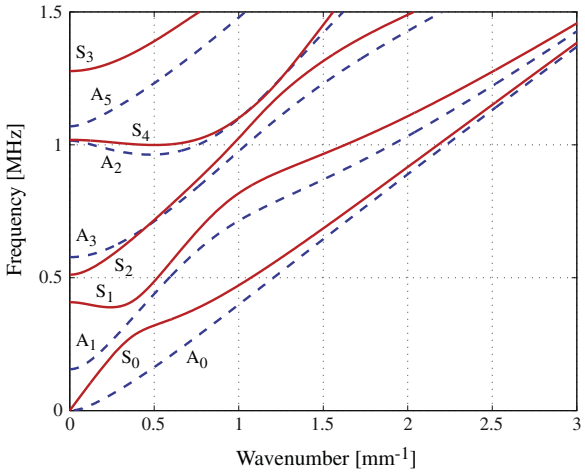

Fig. 2. Dispersion diagram for multi-layer structure consisting of 2 aluminium layers (Al 2014-T6, thickness 3 mm) connected with an epoxy based sealant (Hysol EA 9394, thickness 0.25 mm).

3. Wave mode characteristics

A dispersion diagram of the 6.25 mm thick multilayer structure is shown in Fig. 2. The curves were determined using the software Disperse [27] for a 0.25 mm thick sealant layer, with material properties as described in Section 2. The indices of the guided wave modes were defined in analogy with Lamb waves in a single layer plate according to the naming convention from Royer and Dieulesaint [28]: the index corresponds to the number of nodes in the plate thickness at cut-off frequency for in-plane displacement (odd anti-symmetric modes A_{2n+1} and even symmetric modes S_{2n}) and out-of-plane displacement (even anti-symmetric modes A_{2n} and odd symmetric modes S_{2n+1}), where n is an integer greater than or equal to zero.

The selected excitation centre frequency of 1 MHz is above the cut-off frequency of the higher modes, therefore multiple modes can propagate in the plate structure. At this frequency the fundamental anti-symmetric and symmetric modes A_0 and S_0 have phase velocities of 2819 m/s and 2883 m/s, respectively and the two modes show low dispersive behaviour. This is not the case for the higher modes A_1 and S_1 with phase velocities of 3295 m/s and 3852 m/s, respectively. The use of a 1 MHz, 90° angle beam transducer (for steel) for wave excitation leads to a stress field at the interface between the wedge and the specimen surface with a spatial periodicity of approximately 3.0 mm, corresponding to a phase velocity of 3000 m/s. Based on a comparison with the phase velocity of the different modes that can propagate in the multilayer structure, it can be predicted that both fundamental modes as well as the first higher mode A_1 will be excited in the structure. All other modes have a large difference in terms of phase velocity (next closest mode S_1: 28% difference) and are not expected to be significantly excited.

The mode shape of the fundamental modes (A_0 and S_0) and mode A_1 at 1 MHz are illustrated in Fig. 3. The anti-symmetric mode A_0 represents an individual bending deformation of the adherents of the multilayer structure with a rather constant out-of-plane displacement component and an important in-plane displacement gradient in the sealant layer (Fig. 3(a)). For the S_0 mode, the structure is stretched and compressed in the wave propagation direction. The out-of-plane displacement amplitude increases with increasing distance from the median plane of the plate and the sealant layer is subjected to a significant out-of-plane displacement gradient (Fig. 3(b)). The A_1 mode is associated with stretching

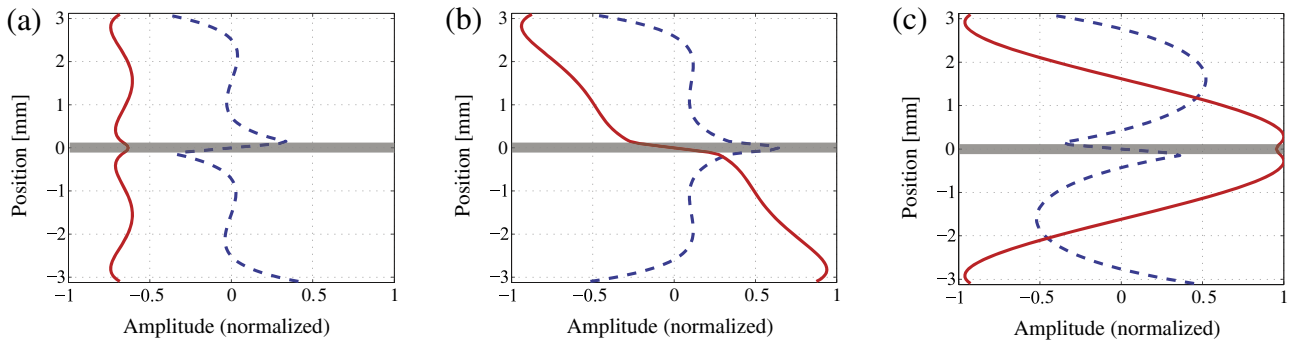

Fig. 3. Mode shapes in multi-layer plate at 1 MHz for: (a) A_0 mode; (b) S_0 mode and (c) A_1 mode; dashed: in-plane; solid: out-of-plane displacement; grey area: sealant layer.

and compression of the individual aluminium plates in the wave propagation direction, but the deformations between upper and lower plates are out-of-phase (Fig. 3(c)). All three modes have significant energy and energy gradient close to the free surfaces and to the sealant layer, thus good sensitivity is expected for surface defects or defects located at the interface between sealant and aluminium.

4. Numerical simulations

The wave propagation in the multilayer structure and the scattering at the notch were simulated using the commercially available software Abaqus/Explicit, based on an explicit dynamic Finite Element (FE) formulation. The numerical investigations were performed with a two-dimensional model representing the side view of the specimen, assuming plane strain wave propagation. For this purpose, a structured mesh was generated using 4 node linear, plane strain, square elements with an element size of 0.05 mm. The element size, corresponding to approximately 1/60 of the wavelength of the fundamental Lamb modes at 1 MHz, was selected to achieve a compromise between numerical dispersion and calculation time. As a general rule, a minimum of ten elements per wavelength are required for correct wave propagation modelling [25]. For Rayleigh or Lamb mode propagation and scattering simulations, the spatial sampling has to be sufficient to reproduce accurately the depth dependence of the stress and displacement fields [26]. In the present contribution, a high accuracy is needed to obtain an accurate simulation of the spatial beating effect between the propagating Lamb modes. Since the beatlength of two modes is inversely proportional to the difference between their wavenumbers [17] and the wave numbers are very close for the two fundamental modes A_0 and S_0, a small numerical error would have a significant impact on the beating effect. The selected element size results in a numerical error below 0.01% for the phase velocity of the fundamental modes and an error below 1% for the corresponding beatlength. The EDM notches were implemented as 0.3 mm deep slots with a flat end, as illustrated in Fig. 1(b), a width of 0.4 mm and stress-free boundary conditions at the surfaces of the defect. Rayleigh damping was used in the FE analysis to account for the measured beam spread and the material damping in the sealant layer (Section 2).

The wave generation was obtained by imposing the in-plane and out-of-plane displacement components (x and z components, respectively, according to the coordinate system in Fig. 1) of the experimentally excited guided ultrasonic wave modes (fundamental modes A_0 and S_0 and the first anti-symmetric mode A_1) on a vertical line through the specimen thickness. The displacement components were determined by addition of the normalized mode shapes at the centre frequency of 1 MHz, obtained with the software Disperse [27], after weighting with the relative mode amplitudes obtained from the measurements. The amplitude ratios were selected to approximately match the average of the experimentally observed wave propagation characteristics as determined from the fitting procedure described in chapter 5.2. As expected, in the vicinity of the upper surface (corresponding to the specimen face on which the 90° angle beam transducer is applied) the resulting displacement profiles were similar to those of a Rayleigh wave. The profiles were multiplied with the excitation signal, a five cycle sinusoid (centre frequency 1 MHz) in a Hanning window, with in-plane and out-of-plane components shifted by a phase angle of $\pi/2$. The calculated, time-dependent displacement components were imposed as boundary conditions on the selected vertical line until the excitation time had elapsed. The nodes adjacent to the excitation line on the side where the wave is not expected to propagate were fixed during excitation in order to prevent the development of a second wave propagating in the opposite direction. The boundary conditions were suppressed after this time to allow for reflections to pass through the excitation line without any disturbance.

The FE simulations of the pulse-echo measurements were performed with a four cycle excitation signal (1 MHz centre frequency) to approximate the observed signal of the angle beam transducer driven by a voltage spike. The received P/E signal for the angle beam transducer was predicted based on the low-dispersive characteristics of the fundamental modes A_0 and S_0. The out-of-plane displacement at the specimen surface was recorded over a monitoring area of 10 mm (50 nodes in 0.2 mm steps) to approximate the interface between the angle beam transducer and the multilayered structure. The predicted pulse-echo signal was obtained by selecting a reference point, phase shifting the predicted time series of the successive points with the Rayleigh wave velocity for steel and summing the resulting time series. This procedure results in an enhancement of the modes with a phase velocity close to the Rayleigh wave velocity as happens in a 90° angle beam transducer [26].

5. Guided wave propagation

5.1. Wave propagation analysis

The measured time series of the out-of-plane displacement component are shown in Fig. 4(a) and (b) for two points situated at 100 mm and 250 mm from the wedge position. The first pulse observed in the time trace remains clear and sharp while propagating, showing the characteristics of low dispersive modes. It matches the two fundamental modes A_0 and S_0 with theoretical group velocities at 1 MHz of 3035 m/s and 2940 m/s respectively. The second pulse propagates slower and stretches in time with the propagation distance due to dispersion, therefore offering less potential for defect detection. It matches the mode A_1 with a theoretical group velocity at 1 MHz of approximately 2170 m/s. The

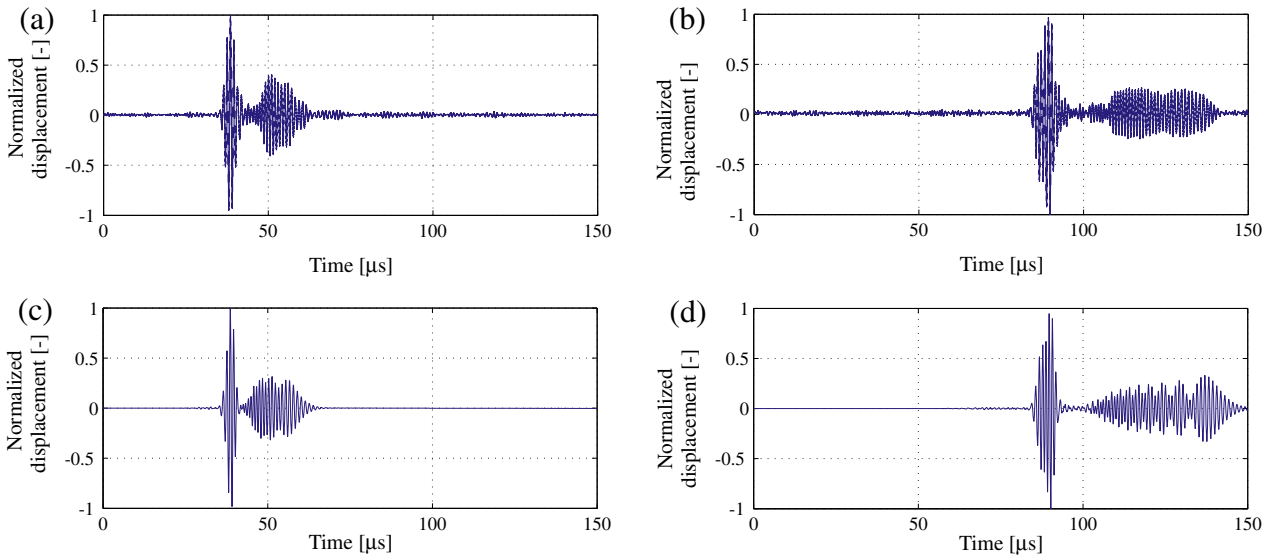

Fig. 4. Time traces of out-of-plane displacement component on free surface of multilayer plate. Measurements: (a) $x = 100$ mm, (b) $x = 250$ mm; FE simulation: (c) $x = 100$ mm, and (d) $x = 250$ mm.

same observations are made from the predicted time series obtained from the FE simulation, illustrated in Fig. 4(c) and (d). The time signals do not match in every detail, but the general shape and amplitude ratios between the pulses show a good overall agreement between the measurements and simulations.

A two-dimensional Fast Fourier Transform (FFT) was used to verify the modes generated by the angle beam transducer. The analysis was performed on displacement time signals measured along the centre line on the excitation side (400 points in 1 mm steps). Three guided wave modes are clearly observable in Fig. 5(a), showing the amplitude as a function of real wavenumber and frequency. A comparison with the theoretical dispersion curves for the multi-layered structure (dashed lines) confirms the fact that the incident wave is dominated by the two fundamental modes A_0, S_0 as well as the antisymmetric mode A_1. A slight offset between the theoretical dispersion curves and the 2D FFT of the measurements can be seen, as the theoretical curves were calculated for nominal material properties and component thicknesses. The same 2D FFT evaluation was applied to the displacement time traces obtained from the FE simulation. Fig. 5(b) shows the good agreement with the theoretical dispersion curves, as the same material and thickness parameters were used.

5.2. Amplitude ratio of excited guided wave modes

The amplitude of the out-of-plane displacement component for each measurement point along the propagation direction was extracted at the centre frequency of 1 MHz using FFT. For this purpose, the incident wave was first isolated from possible reflections by application of a time window propagating with the incident pulse. Size and velocity of the window were selected to include the two fundamental modes A_0 and S_0 and the antisymmetric mode A_1. The evaluation procedure was repeated for each measurement point along the centre line (step size 1 mm) up to a distance of 300 mm from the excitation position. The resulting amplitude curve is displayed in Fig. 6(a) (dashed line). Due to the phase velocity difference between the different modes, constructive and destructive interferences occur and beating effects as described in [17] can be observed. The amplitude variation occurs on two different length scales. The short beating effect with a beat-

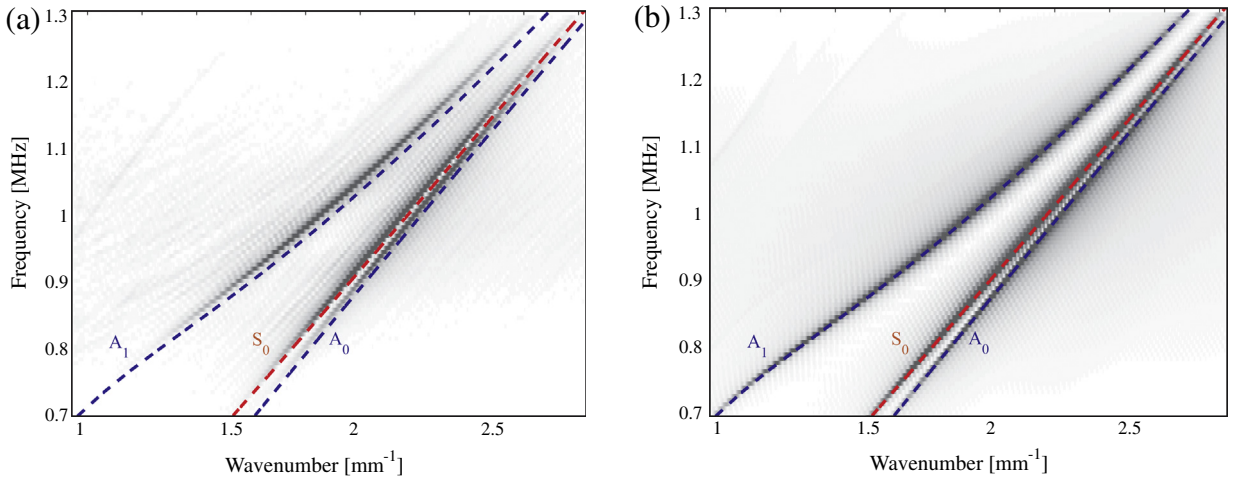

Fig. 5. Two-dimensional FFT amplitude of out-of-plane displacement (400 points on the excitation side in 1 mm steps), with theoretical dispersion curves (dashed): (a) measurements and (b) FE simulation.

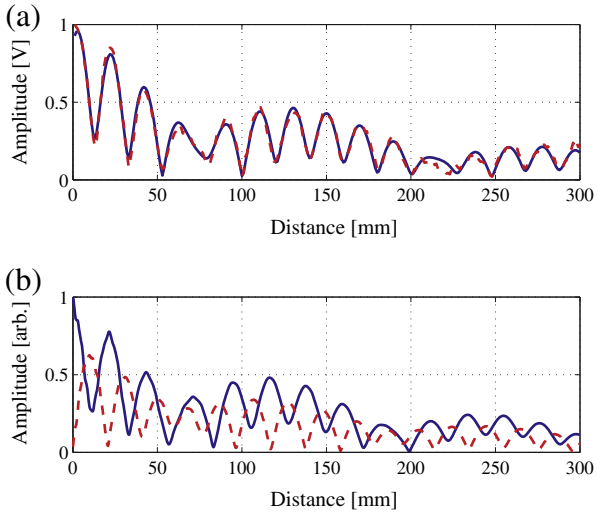

Fig. 6. Out-of-plane displacement amplitude (FFT) at 1 MHz as function of distance on multilayer specimen for interference of A_0, S_0 and A_1 modes: (a) measurement on excitation surface (dashed line) with fitted curve (solid line); (b) FE simulation on excitation surface (solid) and at interface between sealant and aluminium adherent (dashed).

length L of approximately 21 mm is due to the interference of the higher mode A_1 with the fundamental modes A_0 and S_0. The beating effect between A_0 and S_0 with a beatlength of approximately 145 mm is less pronounced.

The experimental curve was fitted using a least square method. The fitting procedure is based on the linear superposition of the three modes at the specimen surface. Based on the theoretical out-of-plane displacement component of each (normalized) mode, the fitting algorithm estimates the coefficient and the phase velocity of each mode, as well as an initial phase shift and an exponential decrease from the initial amplitude due to the combined observed attenuation due to damping and beam spread. For convergence reasons the A_0 phase velocity value was kept constant at a value corresponding to the theoretical prediction. For the resulting fitted curve shown in Fig. 6(a) (solid line), the relative amplitude coefficients were found as 0.57 for the A_0 mode, 0.63 for the S_0 mode and 0.53 for the A_1 mode. These coefficients showed good agreement with the relative amplitude ratios extracted from the two-dimensional FFT presented in Fig. 5.

An investigation of the repeatability of the energy repartition between the excited modes has shown variations which cannot be neglected. The main factor affecting the relative amplitude ratio between the modes appears to be the pattern of the pressure field between the wedge and the specimen. This pressure field mainly depends on the angle-beam transducer and on the couplant and clamping pressure applied on the wedge. For instance, coefficients of 0.34 for A_0, 0.52 for S_0 and 0.79 for A_1 were obtained when using a 90° angle beam transducer from another manufacturer. The influence of the initial A_0 phase velocity value on the coefficients determined using the fitting procedure was found to be negligible. The phase velocities of the three modes and the beatlength values are not significantly affected by the pressure field at the excitation position. For two measurements performed on the same specimen with different angle beam transducers, the phase velocities were found to exhibit a difference of less than 1 m/s (0.03%).

The numerical wave generation in the FE simulations was performed with the following coefficients, based on an average of the measured coefficients: 0.44 for A_0, 0.68 for S_0 and 0.59 for A_1. Fig. 6(b) displays the resulting, predicted out-of-plane displacement amplitude curves on the specimen upper surface (solid line) and at the interface between sealant and upper aluminium layer (dashed line). Despite the difference in terms of coefficients, a comparison between predicted and measured amplitude curves on the upper specimen surface showed good general agreement with similar relative amplitude and interference patterns. The out-of-plane displacement amplitude is generally larger on the upper specimen surface than at the interface between sealant and aluminium layer. This is mainly due to the fact that the out-of-plane displacement component of the S_0 mode, illustrated in Fig. 3(b), is approximately three times larger on the upper specimen surface than at the interface between sealant and aluminium. The evaluation of the simulation curves predicts a beatlength of 129 mm between the A_0 and S_0 modes, very close to the theoretical value calculated using Disperse [27] of 127 mm (error of 1.5%), and in line with the results shown in Fig. 6. This demonstrates that the accuracy of the FE simulation and the numerical dispersion are sufficient to obtain accurate phase velocity values. However, a comparison with the experimentally measured beatlength of approximately 145 mm shows a relative error of 14%. A sensitivity analysis based on Disperse showed that the variation of the sealant layer thickness, which was observed in the specimens, by itself cannot explain the difference in beatlength. It was concluded that the most likely cause is a combination of an incorrect value of the material properties (Young's modulus and Poisson's ratio) and thickness of the sealant layer, which has an opposite influence on the wavenumbers of A_0 and S_0 modes.

5.3. Observed wave propagation and interference

As a more practically relevant observation, the maximum amplitude of the envelope of the time signal along the propagation direction was measured using the Hilbert transform. Apart from the vicinity of the wedge this captures the first pulse in Fig. 4, consisting of the A_0 and S_0 modes. Shown in Fig. 7(a) are the recorded amplitudes (1 mm step size) on the upper (transducer side) and bottom surfaces of two different multilayer specimens. Good repeatability for this practically relevant measurement of the observed pulse amplitude can be seen between the two specimens. The amplitude on the upper surface shows a periodic decrease and increase in line with the long interference length of the A_0 and S_0 modes, with minima at approximately 50 mm and 200 mm, and a maximum at approximately 120 mm. The amplitude curves on

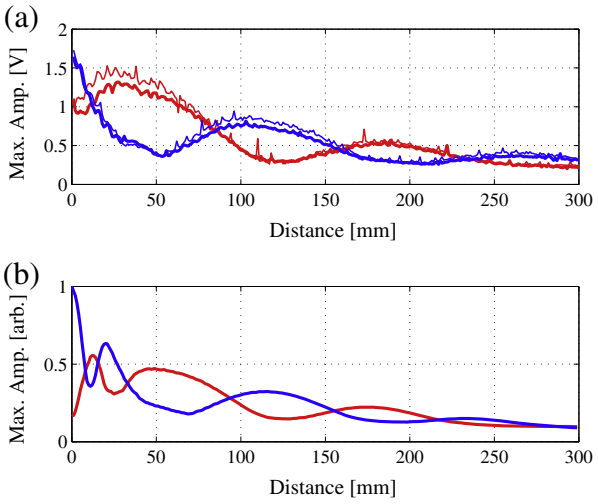

Fig. 7. Maximum amplitude of time traces (Hilbert transform): (a) measurements for 2 specimens; (b) FE simulation; upper surface (transducer side): blue; bottom surface: red. (For interpretation of the references to colour in this figure legend, the reader is referred to the web version of this article.)

the bottom surface show an opposite behaviour with a maximum at about 40 mm from the transducer location and a minimum at about 120 mm. This indicates an energy exchange between the two aluminium plates and thus an insonification of the complete specimen thickness. The overall decrease in amplitude as the wave propagates along the specimen can be attributed to a combination of ultrasonic beam spread, pulse distortion and damping as discussed in Section 2. The amplitude curves resulting from the FE simulation are shown in Fig. 7(b). An additional interference effect close to the excitation position is visible at approximately 10–20 mm. Due to the discussed differences in the beatlength (Section 5.2) the exact locations of the maxima and minima do not match, but in general a good agreement between measured and simulated amplitude curves can be seen in Fig. 7. Overall, a clear guided wave pulse could be observed 300 mm from the transducer location, indicating that this type of high frequency guided ultrasonic wave can be employed for non-destructive testing measurements in a medium range along multi-layered plate specimens.

6. Scattering at a notch

6.1. Numerical prediction of the reflection and transmission coefficients

Initially it was attempted to predict the reflection and transmission coefficients of the different guided waves modes [17] based on an orthogonal modal decomposition of the FE simulation results [9,29]. However, the evaluation of the coefficients in the frequency domain showed a strong variation with small changes in the considered frequency within the bandwidth of the excitation signal. The strong variation can be explained by the presence of three cut-off frequencies in the investigated frequency range: A_2 and S_4 at approximately 1.02 MHz and A_5 at 1.07 MHz, (see Fig. 2). Furthermore, two zero group velocity (ZGV) modes [30] for A_2 and S_4 at 0.96 MHz and 1.0 MHz strongly influence the scattering behaviour. It was therefore decided to concentrate on an evaluation in the time domain, considering only the maximum amplitude of the reflected pulses for the measurements and the FE simulations.

6.2. Defect detection using pulse-echo measurements

The sensitivity for the detection of hidden defects (notch at sealant layer or bottom surface, depth 0.3 mm) was investigated by means of standard ultrasonic pulse-echo measurements. Fig. 8 shows typical time signals for stand-off distances of 150 mm and 300 mm to a notch in the bottom aluminium layer facing the sealant. The excitation, reflection at the notch, and reflection at the plate end can be seen as three different pulses and have amplitude above the noise level in the signal. For 150 mm stand-off distance (Fig. 8(a)), the pulse reflected at the notch is clearly visible at about 120 μs and has about half of the amplitude of the reflection at the plate end at 220 μs. Placing the transducer at 300 mm from the defect, the reflected pulse is reduced in amplitude due to beam spread and material damping of the sealant layer but is still clearly visible at about 220 μs, see Fig. 8(b). The arrival time of the reflection from the notch matches the time-of-flight calculated on the basis of the theoretical group velocity of the A0 and S0 modes for the respective stand-off distance, allowing an approximate localization of the defect.

FE simulations of a pulse-echo measurement were performed for a hidden notch in the aluminium layer facing the sealant. The pulse was obtained by application of the enhancement method described in Section 4. As the wave propagation in the wedge is not simulated the simulation time signals are shifted by 0.02 ms to account for this propagation time. The respective simulated time traces are shown in Fig. 8(c) for 150 mm and Fig. 8(d) for 300 mm standoff distance. Good agreement of the relative arrival times and amplitudes of the pulses can be observed. As observed previously the exact pulse shapes do not match exactly, e.g., the FE simulated reflections at the plate edges show more time separation between the A_0 and S_0 modes. This is most probably due to the slight differences in the measured and theoretical dispersion relations.

As the amplitude values are strongly dependent on the stand-off distance and on the frequency, it was decided to use a detection parameter that can easily be measured in practice: the maximum amplitude of the reflected pulse in the time domain. As the excited guided wave pulse is broadband a reduced amplitude variation with the frequency-dependent beatlength is expected. The influence of the slot location with respect to the specimen thickness

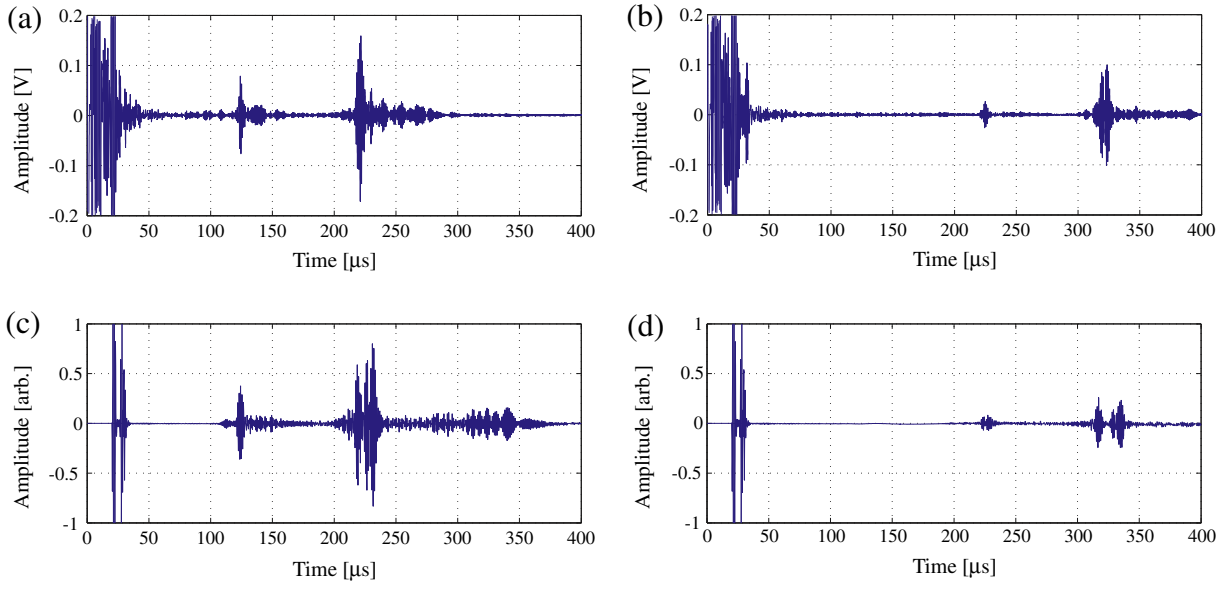

Fig. 8. Pulse-echo time signals using 90° wedge transducer (1 MHz centre frequency), 0.3 mm deep notch in bottom layer facing sealant; measurements (a) 150 mm stand-off distance; (b) 300 mm distance; FE simulations; (c) 150 mm distance; and (d) 300 mm distance.

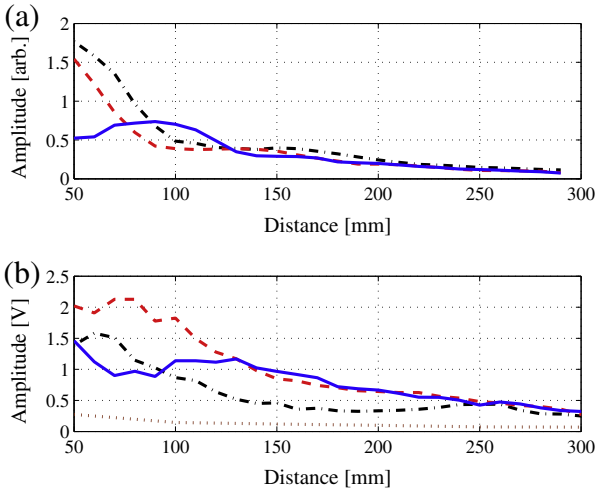

Fig. 9. Maximum amplitude of reflected time signal at 0.3 mm deep notch located in upper layer facing sealant (solid), in bottom layer facing sealant (dashed) and on surface of bottom layer (dash-dotted); (a) FE prediction and (b) pulse-echo measurement (dotted line: noise level).

was investigated by implementing a 0.3 mm deep notch in either the upper or lower aluminium layer at the interface between sealant and metal or as a surface breaking notch on the bottom layer. The resulting amplitude curves are shown in Fig. 9(a). For stand-off distances in a range between 50 mm and 120 mm, the curves for a defect in the bottom layer (dashed and dashed-dot) are characterized by an initial, pronounced amplitude drop leading to a minimum between 100 mm and 150 mm. In fact, in the bottom layer, this location corresponds to a minimum of the amplitude curve resulting from the beating phenomenon between the A_0 and S_0 modes (Fig. 7). For stand-off distances larger than 200 mm, all curves show a similar, monotonic decreasing behaviour.

The amplitude curves resulting from the pulse-echo measurement of a 0.3 mm notch located at the interface between sealant and aluminium and at the bottom specimen surface are shown in Fig. 9(b). Both curves arise from measurements on the same specimen, with notch and excitation in the same aluminium layer (solid) or notch and excitation on opposite aluminium layers (dashed). A comparison with the simulation results in Fig. 9(a) shows similarities of the curve behaviour. The stand-off distance corresponding to the maximum or the minimum amplitude for the notch in the same or in the opposite aluminium layer, respectively, is larger than predicted. This is due to the difference between simulation and measurements for the long beatlength, discussed in Section 4.

The P/E amplitude curve for a surface breaking notch on the bottom layer (dash-dotted) shows similar behaviour to the FE simulations, but has lower amplitude than for the internal defect in the bottom layer. A repeatability study of the pulse-echo measurements has shown that, for the same specimen, the behaviour of the amplitude curve is not significantly affected by parameters such as pressure distribution between the wedge and the specimen. This is not the case for different specimens or transducers where the ratio between the generated modes can be quite different, yielding significant amplitude differences. However, the selection of the maximum amplitude of the time series as detection parameter allows for a minimization of this effect. An estimation of the maximum noise level was performed on the basis of all measurement data and plotted in Fig. 9(b) as reference line (dotted line). For the range of stand-off distances investigated in this work (up to 300 mm), the amplitude of the pulse-echo signal from the defect was always significantly above the noise level, confirming that all defects could be clearly detected from the time traces of the P/E measurements (Fig. 8).

7. Conclusions

The propagation of high-frequency guided ultrasonic waves in multilayer model aerospace structures has been investigated with a view to the non-destructive detection of hidden defects. The considered uniform multilayer component consists of two aluminium plates with a sealant layer. Using single sided access with a standard 90° angle beam wedge transducer guided wave modes were excited that penetrate through the complete thickness of the structure. The wave propagation characteristics were measured experimentally using a laser interferometer and analysed using Fourier transform. The strong, non-dispersive first pulse was identified as the superposition of the fundamental A_0 and S_0 modes, leading to an interference pattern and energy variation along the propagation direction. Additionally the dispersive higher A_1 mode was excited with substantial amplitude due to the similarities in phase velocity, but can be separated in the time domain analysis due to the lower group velocity. The observed wave propagation and pulse shape in the time domain showed good agreement with theoretical predictions and 2D FE simulations. A small difference in the interference pattern (beatlength) most probably results from inaccuracies in the simulation parameters for the sealant layer thickness and material properties. The sensitivity for the detection of small, internal or hidden defects in the metallic adherents facing the sealant layer was predicted from the FE simulations and verified using standard P/E measurements. Good sensitivity was found experimentally for the detection of a small notch cut into the bottom (2nd) layer of the structure with single-sided access limited to the upper surface at a significant standoff distance. Further measurements and simulations will be necessary to better understand the interaction of the high frequency guided waves with real fatigue damage at inaccessible, safety–critical areas and to quantify and verify the sensitivity and maximum achievable standoff distance for the remote detection of hidden damage in multilayer aerospace structures.

Acknowledgement

The authors gratefully acknowledge financial support from the University of Applied Sciences Western Switzerland (HES-SO), Grant 27116.

References

[1] R.P. Dalton, P. Cawley, M.J.S. Lowe, The potential of guided waves for monitoring large areas of metallic aircraft fuselage structures, J. Nondestr. Eval. 20 (2001) 29–46.
[2] J.E. Michaels, T.E. Michaels, B. Mi, An ultrasonic angle beam method for in situ sizing of fastener hole cracks, J. Nondestruct. Eval. 25 (2006) 3–16.
[3] A.C. Cobb, J.E. Michaels, T.E. Michaels, An automated time-frequency approach for ultrasonic monitoring of fastener holes, NDT & E Int. 40 (2007) 525–536.
[4] D.N. Alleyne, P. Cawley, The interaction of Lamb waves with defects, IEEE Trans. Ultrason. Ferroelectr. Freq. Control 39 (1992) 381–397.
[5] D.A. Cook, Y.H. Berthelot, Detection of small surface-breaking cracks in steel using scattering of Rayleigh waves, NDT & E Int. 34 (2001) 483–492.
[6] J.D. Achenbach, A.K. Gautesen, D.A. Mendelsohn, Ray analysis of surface-wave interaction with an edge crack, IEEE Trans. Sonics Ultrason. 27 (1980) 124–129.
[7] M. Hirao, H. Fukuoka, Y. Miura, Scattering of Rayleigh surface waves by edge cracks: numerical simulation and experiment, J. Acoust. Soc. Am. 72 (1982) 602–606.
[8] P. Fromme, P.D. Wilcox, M.J.S. Lowe, P. Cawley, On the development and testing of a guided ultrasonic wave array for structural integrity monitoring, IEEE Trans. Ultrason. Ferroelectr. Freq. Control 53 (2006) 777–785.
[9] M. Castaings, E. Le Clezio, B. Hosten, Modal decomposition method for modeling the interaction of Lamb waves with cracks, J. Acoust. Soc. Am. 112 (2002) 2567–2582.
[10] M.J.S. Lowe, P. Cawley, J.Y. Kao, O. Diligent, The low frequency reflection characteristics of the fundamental antisymmetric Lamb wave a_0 from a rectangular notch in a plate, J. Acoust. Soc. Am. 112 (2002) 2612–2622.
[11] R. Seifried, L.J. Jacobs, J. Qu, Propagation of guided waves in adhesive bonded components, NDT & E Int. 35 (2002) 317–328.

[12] P. Fromme, M.B. Sayir, Measurement of the scattering of a Lamb wave by a through hole in a plate, J. Acoust. Soc. Am. 111 (2002) 1165–1170.
[13] P. Fromme, M.B. Sayir, Detection of cracks at rivet holes using guided waves, Ultrasonics 40 (2002) 199–203.
[14] N. Terrien, D. Osmont, D. Royer, F. Lepoutre, A. Déom, A combined finite element and modal decomposition method to study the interaction of Lamb modes with micro-defects, Ultrasonics 46 (2007) 47–78.
[15] D.W. Greve, P. Zheng, I.J. Oppenheim, The transition from Lamb waves to longitudinal waves in plates, Smart Mater. Struct. 17 (2008) 035029.
[16] I.A. Viktorov, Rayleigh and Lamb Waves, Plenum Press, New York, 1967, pp. 93–96.
[17] B. Masserey, P. Fromme, On the reflection of coupled Rayleigh-like waves at surface defects in plates, J. Acoust. Soc. Am. 123 (2008) 88–98.
[18] B. Masserey, P. Fromme, Surface defect detection in stiffened plate structures using Rayleigh-like wave, NDT & E Int. 42 (2009) 564–572.
[19] B. Masserey, P. Fromme, Fatigue crack growth monitoring using high frequency guided waves, Struct. Health Monit. 12 (5–6) (2013) 484–493.
[20] C.D. Smith, Nondestructive Evaluation of Aging Aircraft, Airports and Aerospace Hardware, in: R.D. Kempt, A.L. Broz (Eds.), Proc. of SPIE 2945, 1996, pp. 200–209.
[21] R.A. Smith, D. Edgard, L.D. Jones, D.M. Percivall, An ultrasonic solution for second-layer crack detection, Insight 47 (2005) 81–84.
[22] E. Kostson, P. Fromme, Fatigue crack growth monitoring in multi-layered structures using guided ultrasonic waves, J. Phys.: Conf. Ser. 195 (2009) 012003.
[23] E. Lindgren, J.C. Aldrin, K. Jata, B. Scholes, J. Knopp, Ultrasonic Plate Waves for Fatigue Crack Detection in Multi-Layered Metallic Structures, in: T. Kundu, (Ed.), Proc. of SPIE 6532, Health Monitoring of Structural and Biological Systems, 2007, p. 653207.
[24] A. Semoroz, B. Masserey, P. Fromme, Monitoring of Hidden Damage in Multi-Layered Aerospace Structures Using High Frequency Guided Waves, in: T. Kundu, (Ed.), Proc. of SPIE 7984, Health Monitoring of Structural and Biological Systems, 2011, p. 79840T.
[25] J. Virieux, P-SV wave propagation in heterogeneous media: velocity–stress finite-difference method, Geophysics 51 (1986) 889–901.
[26] B. Masserey, E. Mazza, Analysis of the near-field ultrasonic scattering at a surface crack, J. Acoust. Soc. Am. 118 (2005) 3585–3594.
[27] B. Pavlakovic, M. Lowe, D. Alleyne, P. Cawley, DISPERSE: A General Purpose Program for Creating Dispersion curves, in: D.O. Thompson, D. Chimenti, (Eds.), Rev. of Prog. in QNDE 16, Plenum, New York, 1997, pp. 185–192.
[28] D. Royer, E. Dieulesaint, Elastic Waves in Solids 1: Free and Guided Propagation, Springer, Berlin, 1999, p. 317.
[29] B.A. Auld, Acoustic Fields and Waves in Solids, vol. 2, Wiley, New York, 1973.
[30] C. Prada, D. Clorennec, D. Royer, Local vibration of an elastic plate and zero-group velocity Lamb modes, J. Acoust. Soc. Am. 124 (2008) 203–212.